Experimental evaluation of the acoustic properties of stacked-screen regenerators

Yuki Ueda[a)]
Department of Bio-Applications and Systems Engineering, Tokyo University of Agriculture and Technology, Nakacho 2-24-16, Koganei, Tokyo 187-8588, Japan

Toshihito Kato and Chisachi Kato
Institute of Industrial Science, The University of Tokyo, Komaba, Meguroku, Tokyo 153-8505, Japan

(Received 13 July 2008; revised 17 November 2008; accepted 2 December 2008)

The experimental evaluation of the wave number and characteristic impedance of stacked-screen regenerators is described. First, a two-by-two transfer matrix of a stacked-screen regenerator was estimated from pressure measurements performed at four different positions; then, the wave number and characteristic impedance of the regenerator were evaluated using a "capillary-tube-based" theory that models a stacked-screen regenerator as an array of pores having a uniform cross section. The evaluation was applied to seven types of stacked-screen regenerators. The experimental results show that these stacked-screen regenerators can be modeled as arrays of circular-cross-section tubes. Moreover, an empirical equation used to estimate the radius of the circular cross section of the tubes comprising the modeled stacked-screen regenerators was addressed.
 [DOI: 10.1121/1.3056552]

PACS number(s): 43.35.Ud, 43.20.Mv [RR] Pages: 780–786

I. INTRODUCTION

The thermal interaction between solid walls and oscillating gas causes a rich variety of thermoacoustic phenomena. By harnessing thermoacoustic phenomena, one can construct thermoacoustic engines and coolers.[1] Thermoacoustic engines and coolers have high reliability because they have no or a few moving parts. Moreover, recently developed thermoacoustic engines and coolers employ a thermodynamic cycle similar to the Stirling cycle; therefore, they have the potential to achieve high efficiency comparable to that of conventional Stirling engines and coolers.[2–5] Due to their high reliability and potential, thermoacoustic devices have attracted much attention.

In thermoacoustic devices based on the Stirling cycle, regenerators comprising stacked screens are usually adopted as an energy conversion component. Hence, in order to design such devices, one must know the characteristics of stacked-screen regenerators. These regenerators can be acoustically characterized by the wave number and the characteristic impedance in them.[6–8] Although the wave number and the characteristic impedance for simple geometries such as arrays of circular- or square-cross-section tubes can be analytically calculated, it is difficult to analytically calculate the wave number and characteristic impedance for stacked-screen regenerators. This is because the flow channels in stacked-screen regenerators are very complex.

In this study, we consider seven types of stacked-screen regenerators and experimentally evaluate their wave number and characteristic impedance. The evaluation is based on a capillary-tube-based theory,[9] which models a stacked-screen regenerator as an array of tubes having a simple geometrical cross section. The experimental results show that a stacked-screen regenerator can be modeled as an array of circular-cross-section tubes and that the wave number and characteristic impedance of a stacked-screen regenerator can be estimated by using the theoretical results of these tubes. Further, a method is discussed that can be used to estimate the radius of the circular cross section of the tubes constituting the model of a stacked-screen regenerator.

In the next section, the theory for the experimental evaluation of the wave number and characteristic impedance is described. In Sec. III, the experimental setup and procedure are explained. In Sec. IV, the preliminary measurements that demonstrate the validity of our evaluation method are shown; then, the experiments performed on stacked-screen regenerators are presented. In Sec. V, the experimental results are discussed. The study is summarized in Sec. VI.

II. THEORY

A. Wave number and characteristic impedance

With Rott's acoustic approximation,[1,10] the momentum and continuity equations for a tube can be written as

$$\frac{dP}{dx} = -\frac{1}{S}\frac{i\omega\rho_m}{1-\chi_\nu}U, \tag{1}$$

$$\frac{dU}{dx} = -\frac{i\omega S[1+(\gamma-1)\chi_\alpha]}{\gamma P_m}P + \frac{\chi_\alpha-\chi_\nu}{(1-\chi_\nu)(1-\sigma)}\frac{1}{T_m}\frac{dT_m}{dx}U, \tag{2}$$

where P is the oscillatory pressure, U is the volume velocity, ω is the angular frequency of pressure oscillations, and S is the cross-sectional area of the tube. ρ_m, P_m, T_m, γ, and σ are

a)Electronic mail: uedayuki@cc.tuat.ac.jp

the mean density, the mean pressure, the mean temperature, the ratio of specific heats, and the Prandtl number of the working gas, respectively. χ_α and χ_ν are the thermoacoustic functions[10,11] that allow us to describe the three-dimensional phenomena in the acoustical channel using the two one-dimensional equations.

It is possible to analytically determine the thermoacoustic functions in a tube having a simple geometrical cross section such as circular and square. In order to express the thermoacoustic functions, we use two parameters: thermal relaxation time τ_α and viscous relaxation time τ_ν.[11] They are defined as

$$\tau_\alpha = r^2/(2\alpha), \tag{3a}$$

$$\tau_\nu = r^2/(2\nu), \tag{3b}$$

where r is the characteristic length in a tube, α is the thermal diffusivity of the working gas, and ν is its kinematic viscosity. For the case of a circular-cross-section tube, r is the radius of its cross section, and for the case of a square-cross-section tube, r is half the side length of its cross section. For the case of a circular-cross-section tube, the thermoacoustic functions χ_α and χ_ν are expressed as[1,10]

$$\chi_\alpha = \frac{2J_1(Y_\alpha)}{Y_\alpha J_0(Y_\alpha)}, \tag{4a}$$

$$\chi_\nu = \frac{2J_1(Y_\nu)}{Y_\nu J_0(Y_\nu)}, \tag{4b}$$

where

$$Y_\alpha = (i-1)\sqrt{\omega\tau_\alpha}, \tag{5a}$$

$$Y_\nu = (i-1)\sqrt{\omega\tau_\nu}. \tag{5b}$$

For the case of a square-cross-section tube,[1,12]

$$\chi_\alpha = 1 - \frac{64}{\pi^4}\sum_{m,n\ \mathrm{odd}}\frac{1}{m^2n^2C_{\alpha,mn}}, \tag{6a}$$

$$\chi_\nu = 1 - \frac{64}{\pi^4}\sum_{m,n\ \mathrm{odd}}\frac{1}{m^2n^2C_{\nu,mn}}, \tag{6b}$$

where

$$C_{\alpha,mn} = 1 - i\frac{\pi^2}{8\omega\tau_\alpha}(m^2+n^2), \tag{7a}$$

$$C_{\nu,mn} = 1 - i\frac{\pi^2}{8\omega\tau_\nu}(m^2+n^2). \tag{7b}$$

Equations (1) and (2) can be solved analytically for a tube with a uniform cross section and with $dT_m/dx=0$, and their solution is expressed by using the wave number k and the characteristic impedance Z_c as

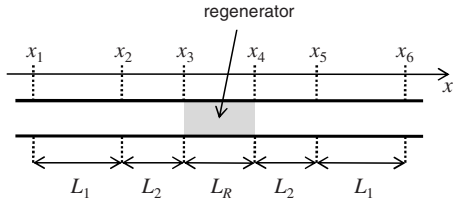

FIG. 1. Coordinate system for the experimental evaluation of the wave number and characterstic impedance for a stacked-screen regenerator.

$$\begin{pmatrix} P_1 \\ U_1 \end{pmatrix} = M(x_1,x_0)\begin{pmatrix} P_0 \\ U_0 \end{pmatrix},$$

$$M(x_1,x_0) \equiv \begin{pmatrix} \cos(k(x_1-x_0)) & \dfrac{Z_c}{iS}\sin(k(x_1-x_0)) \\ \dfrac{S}{iZ_c}\sin(k(x_1-x_0)) & \cos(k(x_1-x_0)) \end{pmatrix}, \tag{8}$$

where P_j and U_j represent the oscillatory pressure and volume velocity at x_j, respectively. The wave number k and the characteristic impedance Z_c are written by using the thermoacoustic functions as

$$k = k_0\sqrt{\frac{1+(\gamma-1)\chi_\alpha}{1-\chi_\nu}} \tag{9}$$

and

$$Z_c = Z_0\frac{k_0}{k(1-\chi_\nu)}, \tag{10}$$

where $k_0=\omega/a$ and $Z_0=\rho_m a$, respectively; a is the adiabatic sound speed.

B. Theory for measurements

In this subsection, we describe the theory used for the experimental evaluation of the wave number k_{exp} and the characteristic impedance $Z_{c\mathrm{exp}}$ for a stacked-screen regenerator. In this theory, the transfer-matrix method[7,8,13] is used, and the capillary-tube-based theory[9] that models a stacked-screen regenerator as an array of pores having a uniform cross section is employed.

We consider the case wherein the regenerator of a length L_R is sandwiched between two circular-cross-section tubes, as shown in Fig. 1. The k and Z_c values in these tubes can be calculated from Eqs. (4), (9), and (10) and are denoted as k_T and $Z_{c,T}$, respectively. The axial coordinate x and the lengths L_1, L_2, and L_R are set as shown in Fig. 1.

By using Eq. (8), the oscillatory pressure and volume velocity at $x=x_1$, (P_1,U_1), can be related to those at x_2, (P_2,U_2),

$$\begin{pmatrix} A_a & B_a \\ C_a & A_a \end{pmatrix}\begin{pmatrix} P_1 \\ U_1 \end{pmatrix} = \begin{pmatrix} P_2 \\ U_2 \end{pmatrix}, \tag{11}$$

where

$$A_a = \cos k_T L_1, \tag{12}$$

$$B_a = \frac{Z_{c,T}}{iS_T} \sin k_T L_1, \tag{13}$$

$$C_a = \frac{S_T}{iZ_{c,T}} \sin k_T L_1. \tag{14}$$

Here, $L_1 = x_2 - x_1 (= x_6 - x_5)$ and S_T is the cross-sectional area of the tubes. The pressure P_2 and volume velocity U_2 at $x = x_2$ can be related to the pressure P_3 and volume velocity U_3 at one end of the regenerator, $x = x_3$,

$$\begin{pmatrix} A_b & B_b \\ C_b & A_b \end{pmatrix} \begin{pmatrix} P_2 \\ U_2 \end{pmatrix} = \begin{pmatrix} P_3 \\ U_3 \end{pmatrix}, \tag{15}$$

where

$$A_b = \cos k_T L_2, \tag{16}$$

$$B_a = \frac{Z_{c,T}}{iS_T} \sin k_T L_2, \tag{17}$$

$$C_a = \frac{S_T}{iZ_{c,T}} \sin k_T L_2. \tag{18}$$

Here, $L_2 = x_3 - x_2 (= x_5 - x_4)$. Equation (11) yields

$$U_1 = (P_2 - A_a P_1)/B_a, \tag{19}$$

$$U_2 = C_a P_1 + A_a U_1. \tag{20}$$

By using Eqs. (15), (19), and (20), we obtain

$$P_3 = A_b P_2 + B_b \left(C_a P_1 + \frac{A_a}{B_a} (P_2 - A_a P_1) \right), \tag{21}$$

$$U_3 = C_b P_2 + A_b \left(C_a P_1 + \frac{A_a}{B_a} (P_2 - A_a P_1) \right). \tag{22}$$

Following the above approach, the following two equations are obtained:

$$P_4 = A_b P_5 + B_b \left(C_a P_6 + \frac{A_a}{B_a} (P_5 - A_a P_6) \right), \tag{23}$$

$$U_4 = -C_b P_5 - A_b \left(C_a P_6 + \frac{A_a}{B_a} (P_5 - P_a P_6) \right), \tag{24}$$

where P_4 and U_4 are the pressure and volume velocity at the other end of the regenerator, $x = x_4$.

Although the wave number k_{exp} and the characteristic impedance $Z_{c,\mathrm{exp}}$ for the regenerator are still unknown, the relation between (P_3, U_3) and (P_4, U_4) can be written as

$$\begin{pmatrix} A_R & B_R \\ C_R & A_R \end{pmatrix} \begin{pmatrix} P_3 \\ U_3 \end{pmatrix} = \begin{pmatrix} P_4 \\ U_4 \end{pmatrix}, \tag{25}$$

where

$$A_R = \cos k_{\mathrm{exp}} L_R, \tag{26}$$

$$B_R = \frac{Z_{c,\mathrm{exp}}}{iS_R} \sin k_{\mathrm{exp}} L_R, \tag{27}$$

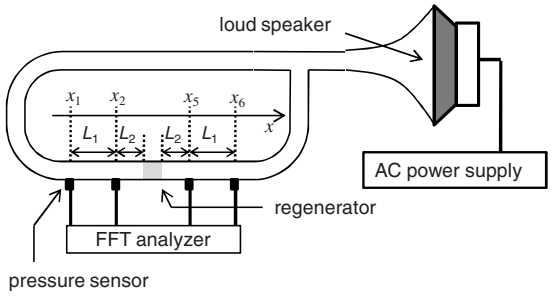

FIG. 2. Experimental setup to evaluate the wave number and characteristic impedance for a stacked-screen regenerator.

$$C_R = \frac{S_R}{iZ_{c,\mathrm{exp}}} \sin k_{\mathrm{exp}} L_R, \tag{28}$$

and S_R is the cross-sectional area of the regenerator. This is because the regenerator is modeled as an array of pores having a uniform cross section. Since the determinant of the matrix in Eq. (25) is unity, i.e., $A_R^2 - B_R C_R = 1$,

$$\begin{pmatrix} A_R & -B_R \\ -C_R & A_R \end{pmatrix} \begin{pmatrix} P_4 \\ U_4 \end{pmatrix} = \begin{pmatrix} P_3 \\ U_3 \end{pmatrix}. \tag{29}$$

Equations (25) and (29) yield

$$A_R = \frac{P_3 U_3 + P_4 U_4}{P_3 U_4 + P_4 U_3}, \tag{30}$$

$$B_R = \frac{P_4^2 - P_3^2}{P_4 U_3 + P_3 U_4}, \tag{31}$$

$$C_R = \frac{U_4^2 - U_3^2}{P_4 U_3 + P_3 U_4}. \tag{32}$$

From Eqs. (26) and (30), we obtain

$$k_{\mathrm{exp}} = \left(\arccos \left(\frac{P_3 U_3 + P_4 U_4}{P_3 U_4 + P_4 U_3} \right) \right) \Big/ L_R, \tag{33}$$

and from Eqs. (27), (28), (31), and (32), we obtain

$$Z_{c,\mathrm{exp}} = S_R \sqrt{\frac{P_4^2 - P_3^2}{U_4^2 - U_3^2}}. \tag{34}$$

Equations (33) and (34) indicate the following: when a stacked-screen regenerator is sandwiched by the circular tubes for which Z_c and k are analytically calculated, the pressure measurements at four positions allow us to evaluate the wave number and characteristic impedance for the regenerator. This is because (P_3, U_3) and (P_4, U_4) in Eq. (33) can be expressed by the matrix elements $(A_a, B_a, C_a, A_b, B_b, C_b)$ and the four values of pressure (P_1, P_2, P_5, P_6), as can be seen in Eqs. (21)–(24).

III. EXPERIMENTAL SETUP AND PROCEDURE

The constructed experimental setup is shown in Fig. 2. It was composed of a loudspeaker, branching resonator, looped tube, and regenerator. The looped tube was used to make the phase difference between measured pressures large enough to be measured. A regenerator having a length of L_R

=20 mm was inserted into the looped tube. The lengths of the looped tube and branching resonator were 2.5 m and between 0.5 and 1.0 m, respectively, and their inner diameter was 24 mm. The tube and resonator were filled with atmospheric air.

We constructed the stacked-screen regenerators by randomly stacking stainless-steel wire mesh screens. The diameter of the screen wire is denoted as d. Half the hydraulic diameter $(D_h/2)$ is employed as the characteristic radius r of a stacked-screen regenerator. D_h is defined as the value that is four times the ratio of the gas volume V_{gas} to the gas-solid contact surface area $S_{g\text{-}s}$ in a stacked-screen regenerator, i.e.,

$$D_h = \frac{4V_{\mathrm{gas}}}{S_{g\text{-}s}}. \tag{35}$$

V_{gas} is calculated from the equation $V_{\mathrm{gas}}=V_{\mathrm{holder}}-V_{\mathrm{solid}}$, where V_{holder} denotes the volume of the regenerator holder and V_{solid} denotes the volume of the wires of a stacked-screen regenerator. $S_{g\text{-}s}$ is estimated from the surface area of the wires and the inner-side surface area of the regenerator holder. For the evaluation of $Z_{c,\mathrm{exp}}$, the cross-sectional area S_R of a stacked-screen regenerator is required [see Eq. (34)]. However, in a stacked-screen regenerator, flow channels are not uniform along the axial direction, and hence, S_R is also nonuniform. Hence, instead of S_R, we use the porosity ϵ of a regenerator for the evaluation; ϵ is defined as $\epsilon=V_{\mathrm{gas}}/V_{\mathrm{holder}}$.

Four pressure sensors (Toyodakoki DD-102 whose resonant frequency is 5 kHz) were mounted on the wall of the looped tube. The distance between the positions of the mounted pressure sensors, L_1 (see Fig. 2), was set to 0.30 m, and the distance of the mounted pressure sensor from the regenerator, L_2 (see Fig. 2), was 0.10 m. We used a 24 bit fast Fourier transform analyzer (Ono sokki DS-2000 whose maximum sampling frequency is 102.4 kHz) to analyze the signal received from the pressure sensors. When oscillatory pressure was measured with the four pressure sensors located at the same axial position and the measured signals were input to the fast Fourier transform analyzer, the obtained phase and amplitude differences between the measured pressure signals were found to be smaller than 0.1° and 0.5%, respectively.

Alternating-current power was continuously supplied to the loudspeaker, and the pressure oscillation was measured at four positions x_1, x_2, x_5, and x_6 (see Fig. 2). By substituting the measured pressures P_1, P_2, P_5, and P_6 into Eqs. (21)–(24), the pressure and volume velocity at both ends of the regenerator were calculated. By substituting the calculated pressure and volume velocity into Eqs. (33) and (34), we evaluated the wave number k_{exp} and characteristic impedance $Z_{c,\mathrm{exp}}$. The regenerator was air cooled so that the temperature gradient along the regenerator was not caused by the thermoacoustic effect.[4] The measurements were made under the condition that the pressure amplitude is sufficiently small to avoid nonlinear effects.

TABLE I. Geometrical properties of the ceramic honeycombs. D_h denotes hydraulic diameter.

Type	SA	SB	SC	SD
$D_h=2r$ (mm)	0.66	0.75	0.90	1.36
Porosity ϵ (%)	87	85	83	69

IV. EXPERIMENTAL RESULTS

A. Preliminary measurements

Preliminary measurements were performed to check our implementation of the present evaluation method of the wave number and characteristic impedance. In these measurements, ceramic honeycombs having many square-cross-section pores were used as regenerators.

We used four types of ceramic honeycombs. Their properties are listed in Table I. The values of D_h were calculated from Eq. (35). Since the ceramic honeycombs can be regarded as arrays of tubes having a uniform square cross section, the wave number k and the characteristic impedance Z_c can be analytically obtained from Eqs. (6), (9), and (10): The theoretically obtained wave number and the characteristic impedance are denoted as k_{theo} and $Z_{c,\mathrm{theo}}$, respectively.

The measurements were made in a frequency range from 40 to 490 Hz and were repeated four times at a given frequency for each ceramic honeycomb. Figures 3 and 4 show the experimentally obtained wave number k_{exp} and characteristic impedance $Z_{c,\mathrm{exp}}$, respectively; the symbols and error bars indicate the mean value and standard deviation of the four measurements, respectively. Note that k_{exp} and $Z_{c,\mathrm{exp}}$ are divided by $k_0=\omega/a$ and $Z_0=\rho_m a$, respectively, where a is the adiabatic sound speed. The theoretically obtained dimensionless wave number k_{theo}/k_0 and characteristic impedance $Z_{c,\mathrm{theo}}/Z_0$ are also shown by dotted lines in Figs. 3 and 4, respectively.

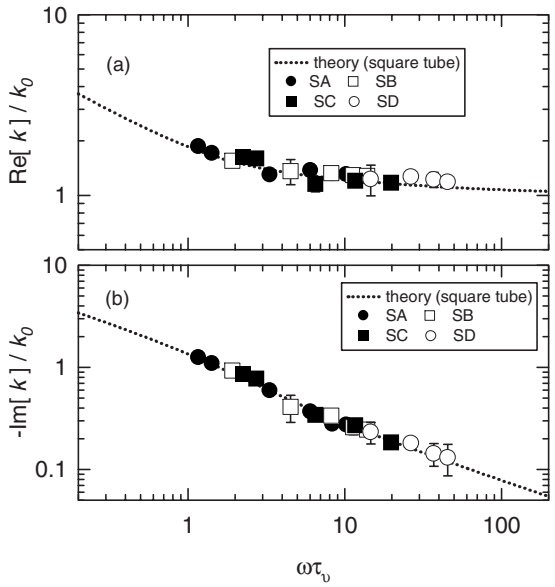

FIG. 3. The experimental results of the dimensionless wave number k/k_0 of the ceramic honeycombs. The experimental results are shown by symbols, and the theoretical results for a square-cross-section tube are shown by dotted lines.

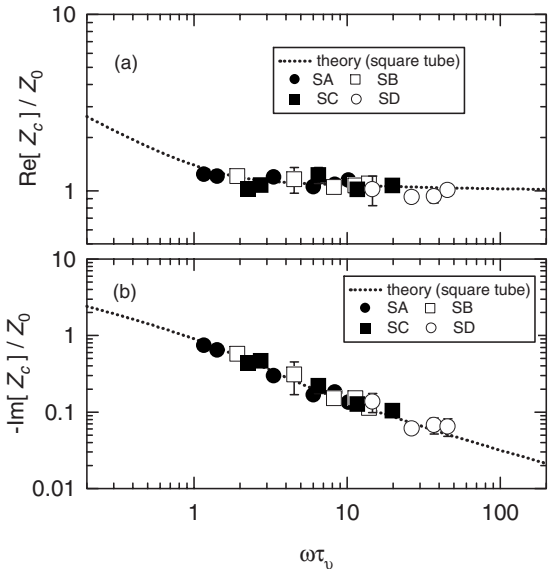

FIG. 4. The experimental results of the dimensionless characteristic impedance Z_c/Z_0 of the ceramic honeycombs. The experimental results are shown by symbols, and the theoretical results for a square-cross-section tube are shown by dotted lines.

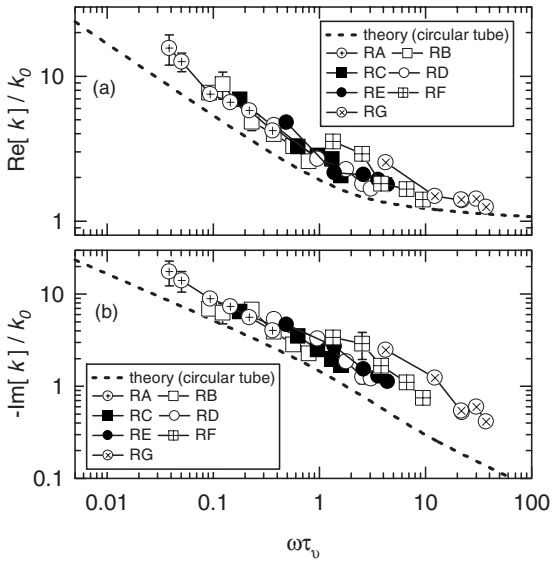

FIG. 5. The experimental results of the wave number k for the stacked-screen regenerators. The dimensionless wave number k/k_0 is shown as a function of $\omega\tau_\nu$.

As can be seen in Fig. 3, the values of the experimentally obtained wave number agree with the theoretical values; the maximum discrepancies between the theoretical and measured mean values of $\mathrm{Re}[k/k_0]$ and those of $\mathrm{Im}[k/k_0]$ are 11% and 15% of the theoretical values, respectively. Figure 4 shows that $Z_{c,\mathrm{exp}}$ agrees with the analytically obtained thermoacoustic function $Z_{c,\mathrm{theo}}$ within a discrepancy of 25% of the theoretical values. On the basis of these results, we consider that the present method can be used for evaluating the wave number k and characteristic impedance Z_c in a stack-screen regenerator.

B. Experimental results with staked screen regenerators

For a stacked-screen regenerator, k_{exp} and Z_c were experimentally evaluated using the method described in Sec. IV A. Seven types of stacked-screen regenerators were used. The geometrical properties of the regenerators are listed in Table II. Note that f_1^2 in this table will be described later.

The experimentally obtained k_{exp}/k_0 of the stacked-screen regenerators is shown as a function of $\omega\tau_\nu$ in Fig. 5. The theoretically obtained wave number k_{theo}/k_0 of a circular-cross-section tube is also shown as a reference. As shown in Fig. 5, $\mathrm{Re}[k_{\mathrm{exp}}/k_0]$ and $-\mathrm{Im}[k_{\mathrm{exp}}/k_0]$ are larger than $\mathrm{Re}[k_{\mathrm{theo}}/k_0]$ and $-\mathrm{Im}[k_{\mathrm{theo}}/k_0]$, respectively, and at a given value of $\omega\tau_\nu$, the values of the real and imaginary parts of k_{exp}/k_0 depend on the type of regenerator. In other words, the wave number of a stacked-screen regenerator depends not only on $\omega\tau_\nu$ but also on the type of regenerator. However, the plots of the real and imaginary parts of k_{exp}/k_0 of each stacked-screen regenerator appear to be parallel to those of k_{theo}/k_0. This implies that by using fitting factors that shift the $\omega\tau_\nu$ versus k_{exp}/k_0 curves toward the $\omega\tau_\nu$ versus k_{theo}/k_0 curves in Fig. 5, the stacked-screen regenerators can be modeled as arrays of circular-cross-section tubes.

The two fitting factors f_1 and f_2 can be used to fit the $\omega\tau_\nu$ versus k_{exp}/k_0 curves to the $\omega\tau_\nu$ versus k_{theo}/k_0 curves.[9,14–17] f_1 and f_2 shift the $\omega\tau_\nu$ versus k_{exp}/k_0 curves toward the left and down in Fig. 5, respectively. However, we introduce only f_1 because we have found that the goodness of fit between the shifted $\omega\tau_\nu$ versus k_{exp}/k_0 curves and the $\omega\tau_\nu$ versus k_{theo}/k_0 curves for each stacked-screen regenerator obtained using only f_1 is almost the same as that obtained using both f_1 and f_2: The goodness of fit for each stacked-screen regenerator was evaluated from the minimum value of the quantity,

TABLE II. Geometrical properties of the stacked-screen regenerators. D_h and f_1^2 denote hydraulic diameter and square of the fitting factor, respectively.

Type	RA	RB	RC	RD	RE	RF	RG
Mesh No.	200	100	80	60		40	24
Wire diameter d (mm)	0.04	0.10	0.10	0.12		0.14	0.22
Porosity (%)	76	66	73	75	78	83	86
$D_h=2r$ (mm)	0.13	0.19	0.26	0.36	0.43	0.65	1.23
f_1^2	2.6	2.1	2.4	2.5	3.2	4.8	6.8

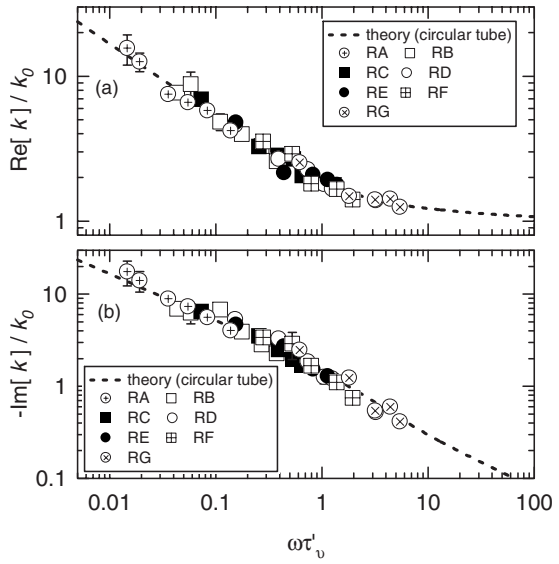

FIG. 6. The experimental results of the wave number k for the stacked-screen regenerators. The dimensionless wave number k/k_0 is shown as a function of $\omega\tau'_\nu=\omega\tau_\nu/f_1^2$.

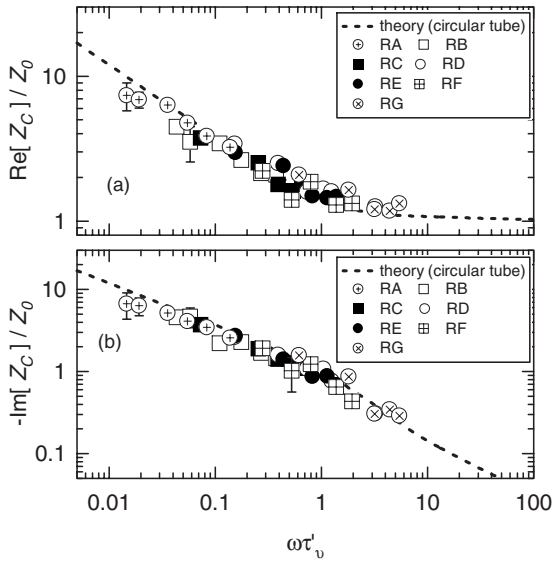

FIG. 7. The experimental results of the characteristic impedance Z for the stacked-screen regenerators. The dimensionless characteristic impedance Z/Z_0 is shown as a function of $\omega\tau'_\nu=\omega\tau_\nu/f_1^2$.

$$F(f_1,f_2)=\sum_{i=1}^{N}\left(\log_{10}\frac{\mathrm{Re}[k_{i,\mathrm{exp}}(\omega\tau'_\nu)]}{f_2\,\mathrm{Re}[k_{i,\mathrm{theo}}(\omega\tau_\nu)]}\right)^2+\sum_{i=1}^{N}\left(\log_{10}\frac{\mathrm{Im}[k_{i,\mathrm{exp}}(\omega\tau'_\nu)]}{f_2\,\mathrm{Im}[k_{i,\mathrm{theo}}(\omega\tau_\nu)]}\right)^2, \tag{36}$$

where

$$\tau'_\nu=\frac{\tau_\nu}{f_1^2} \tag{37}$$

and N is the number of measured data for each stacked-screen regenerator. This would be attributed to the fact that the present measurements were made in the low-$\omega\tau_\nu$ region where both $\mathrm{Re}[k/k_0]$ and $\mathrm{Im}[k/k_0]$ largely depend on $\omega\tau_\nu$, as shown by the dashed lines in Fig. 5.

For each type of the regenerators listed in Table II, f_1^2 was determined so that the value of the goodness of fit $F(f_1)$ is as small as possible. The obtained values of f_1^2 are shown in Table II, and k_{exp}/k_0 and k_{theo}/k_0 are shown as functions of $\omega\tau'_\nu$ in Fig. 6. Note that for the case of k_{theo}, f_1^2 is set to unity, i.e., $\tau'_\nu=\tau_\nu$. Figure 6 shows that the real and imaginary parts of the experimentally obtained wave number k_{exp}/k_0 agree well with those of k_{theo}/k_0. The experimentally determined characteristic impedance $Z_{c,\mathrm{exp}}$ is plotted as a function of $\omega\tau'_\nu$ in Fig. 7. As shown in this figure, the real and imaginary parts of $Z_{c,\mathrm{exp}}/Z_0$ are in acceptable agreement with those of $Z_{c,\mathrm{theo}}/Z_0$; a discrepancy between the measured and theoretical values is within 35% of the theoretical values. From these results, we conclude that stacked-screen regenerators having complex flow channels can be modeled as an array of circular-cross-section tubes by using the obtained values of the fitting factor f_1.

V. DISCUSSION

Table II shows that the fitting factor f_1 largely depends on the type of the regenerator. This indicates that the effective circular radius of the stacked-screen regenerator depends not only on $D_h/2$ but also on its type; the effective circular radius can be defined as

$$r_{\mathrm{eff}}=\sqrt{2\nu\tau'_\nu}=\frac{D_h/2}{f_1}. \tag{38}$$

In this section, the method to estimate the value of f_1 and that of r_{eff} with the characteristics of the stacked-screen regenerators is discussed.

To calculate τ_ν, we employed half the hydraulic diameter $D_h/2$ as the characteristic length r of a stacked-screen regenerator. This is because for the theoretical case of a circular-cross-section tube, the radius of its cross section is used as the characteristic length r and the radius; i.e., r is equal to $D_h/2$. However, for a stacked-screen regenerator, in addition to $D_h/2$, half the wire diameter and half the spacing between the wires that constitute its screens can be regarded as its characteristic lengths; half the wire diameter is approximately equal to half the wire spacing along the axial direction. Hence, we attempt to express f_1 and r_{eff} by using these characteristic lengths.

We focus on the values of the geometric average of 2 or 3 out of $D_h/2$, $d/2$, and $D_s/2$, where d is the wire diameter and D_s is the spacing between wires. D_s can be written as

$$D_s=\frac{25.4\times10^{-3}}{\text{mesh number}}-d. \tag{39}$$

We defined

$$r_1=\frac{\sqrt{D_h d}}{2}, \tag{40}$$

$$r_2=\frac{\sqrt{D_h D_s}}{2}, \tag{41}$$

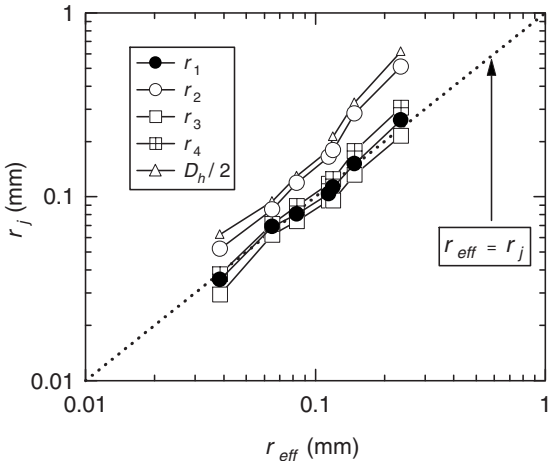

FIG. 8. The relation between r_j and r_{eff} $(j=1,2,3,4)$.

$$r_3 = \frac{\sqrt{D_s d}}{2}, \tag{42}$$

$$r_4 = \frac{\sqrt[3]{D_h D_s d}}{2} \tag{43}$$

and calculated r_j $(j=1,2,3,4)$.

In Fig. 8, r_j is plotted as a function of the experimentally evaluated value of r_{eff} the $r_j=r_{\mathrm{eff}}$ line and D_h versus r_{eff} plot are also shown. As can be seen in this figure, the calculated values of r_1 are closest to the experimentally evaluated values of r_{eff}, and it was found that the difference between r_1 and r_{eff} is smaller than 0.10 of r_{eff}. This indicates that the effective circular radius r_{eff} is approximately expressed by r_1, i.e.,

$$r_{\mathrm{eff}} \approx \frac{\sqrt{D_h d}}{2}, \tag{44}$$

and therefore, the fitting factor f_1 of the stacked-screen regenerators is approximately denoted as

$$f_1 = \frac{D_h/2}{r_{\mathrm{eff}}} \approx \frac{D_h/2}{r_1} = \sqrt{\frac{D_h}{d}}. \tag{45}$$

In other words, the important characteristic length of stacked-screen regenerators is given by the value of the geometric average of its half the hydraulic diameter and half the wire diameter, and the stacked-screen regenerator is approximately modeled as an array of circular-cross-section tubes with the radius of cross section equal to the above characteristic length.

VI. SUMMARY

We have shown the experimental evaluations of the wave number and characteristic impedance for ceramic honeycombs and stacked-screen regenerators. The experimental results of the ceramic honeycombs demonstrated the validity of the present evaluation method. The results of the stacked-screen regenerators indicated that a stacked-screen regenerator can be modeled as an array of circular-cross-section tubes by using one fitting factor f_1, which depends on the type of the regenerator. Further, it was demonstrated that the value of f_1 is approximately estimated by using the hydraulic diameter and the wire diameter of the regenerators.

ACKNOWLEDGMENTS

This research was partially supported by the Ministry of Education, Science, Sports, and Culture in Japan under the Grant-in-Aid for Scientific Research (19860030, 2008) and the Grant-in-Aid for Division of Young Researchers. The authors would like to thank the reviewers for very useful comments and suggestions.

[1]G. W. Swift, *Thermoacoustics: A Unifying Perspective for Some Engines and Refrigerators* (Acoustical Society of America, Melville, NY, 2002).
[2]P. Ceperley, "A piston-less Stirling engine," J. Acoust. Soc. Am. **65**, 1508–1513 (1979).
[3]S. Backhaus and G. W. Swift, "A thermoacoustic Stirling engine," Nature (London) **399**, 335–338 (1999).
[4]G. W. Swift, D. L. Gardner, and S. Backhaus, "Acoustic recovery of lost power in pulse tube refrigerators," J. Acoust. Soc. Am. **105**, 711–724 (1999).
[5]M. Tijani and S. Spoelstra, "Study of a coaxial thermoacoustic-Stirling cooler," Cryogenics **48**, 77–82 (2008).
[6]K. Attenborough, "Acoustical characteristics of rigid fibrous absorbents and granular materials," J. Acoust. Soc. Am. **73**, 785–799 (1983).
[7]R. Muehleisen, C. W. Beamer, IV, and B. Tinianov, "Measurements and empirical model of the acoustic properties of reticulated vitreous carbon," J. Acoust. Soc. Am. **117**, 536–544 (2005).
[8]B. H. Song and J. S. Bolton, "A transfer-matrix approach for estimating the characteristic impedance and wave numbers of limp and rigid porous materials," J. Acoust. Soc. Am. **107**, 1131–1152 (2000).
[9]K. Attenborough, "Acoustical characteristics of porous materials," Phys. Rep. **82**, 179–227 (1982).
[10]N. Rott, "Damped and thermally driven acoustic oscillations," Z. Angew. Math. Phys. **20**, 230–243 (1969).
[11]A. Tominaga, "Thermodynamic aspect of thermoacoustic phenomena," Cryogenics **35**, 427–440 (1995).
[12]W. Arnott, H. Bass, and R. Raspet, "General formulation of thermoacoustics for stacks having arbitrarily shaped pore cross sections," J. Acoust. Soc. Am. **90**, 3228–3237 (1991).
[13]Y. Ueda and C. Kato, "Stability analysis for spontaneous gas oscillations thermally induced in straight and looped tubes," J. Acoust. Soc. Am. **124**, 851–858 (2008).
[14]L. A. Wilen, "Measurements of thermoacoustic functions for single pores," J. Acoust. Soc. Am. **103**, 1406–1412 (1998).
[15]A. Petculescu and L. A. Wilen, "Lumped-element technique for the measurement of complex density," J. Acoust. Soc. Am. **110**, 1950–1957 (2001).
[16]W. Arnott, J. Belcher, R. Raspet, and H. Bass, "Stability analysis of a helium-filled thermoacoustic engine," J. Acoust. Soc. Am. **96**, 370–375 (1994).
[17]H. Roh, R. Raspet, and H. Bass, "Parallel capillary-tube-based extension of thermoacoustic theory for random porous media," J. Acoust. Soc. Am. **121**, 1413–1422 (2007).